electronics

MDPI

Article

Application of Reduced Order Surrogate Models in Compatible Determination of Material Properties Profiles by Eddy Current Method

Volodymyr Y. Halchenko [1], Ruslana Trembovetska [1], Volodymyr Tychkov [1], Viacheslav Kovtun [2,*] and Nataliia Tychkova [1]

[1] Department of Instrumentation, Mechatronics and Computerized Technologies, Cherkasy State Technological University, 460 Shevchenko Blvd., 18006 Cherkasy, Ukraine; v.halchenko@chdtu.edu.ua (V.Y.H.); r.trembovetska@chdtu.edu.ua (R.T.); v.tychkov@chdtu.edu.ua (V.T.); n.b.tychkova.asp21@chdtu.edu.ua (N.T.)

[2] Internet of Things Group, Institute of Theoretical and Applied Informatics, Polish Academy of Sciences, Bałtycka 5, 44-100 Gliwice, Poland

* Correspondence: vkovtun@iitis.pl

Abstract: A number of computer experiments have investigated the effectiveness in terms of accuracy of the method for simultaneously determining the distributions of electrical conductivity and magnetic permeability in the subsurface zone of planar conductive objects when modeling the process of eddy-current measurement testing by surface probes. The method is based on the use of surrogate optimization, which involves the use of a high-performance neural network proxy-model of probe by means of a deep learning as part of the target quadratic function. The surrogate model acts as a carrier and storage of a priori information about the object and takes into account the influence of all the main factors essential in the formation of the probe output signal. The problems of the surrogate model's cumbersomeness and mitigation of the "curse of dimensionality" effect are solved by applying techniques for reducing the dimensionality of the design space based on the PCA algorithm. We investigated options for compromise solutions regarding the dimensionality of the PCA-space and the accuracy of obtaining the desired material properties profiles by the optimization method. The results of modeling the inverse measurement problem indicate a fairly high accuracy of profile reconstruction.

Keywords: material properties; eddy current measurements; surrogate optimization; reduced order metamodel; a priori information; PCA space; deep neural networks

check for updates

Academic Editor: Wojciech M. Zabołotny

Received: 19 November 2024
Revised: 21 December 2024
Accepted: 2 January 2025
Published: 6 January 2025

Citation: Halchenko, V.Y.; Trembovetska, R.; Tychkov, V.; Kovtun, V.; Tychkova, N. Application of Reduced Order Surrogate Models in Compatible Determination of Material Properties Profiles by Eddy Current Method. *Electronics* **2025**, *14*, 212. https://doi.org/10.3390/electronics14010212

1. Introduction

Eddy current analysis of the microstructure of materials is an important tool in many fields of science, engineering, and industry due to its unique properties and the ability to analyze it in detail and detect deviations from the norm.

Magnetic permeability (MP) and electrical conductivity (EC) are highly structure-sensitive parameters of a ferromagnetic material, and knowledge of their surface distributions, i.e., profiles, allows us to track the transformations of its local-spatial physic-mechanical properties, including hardness, plasticity, viscosity, strength, etc., as well as its chemical and phase composition. In the original state, the material of the test objects (TO) is homogeneous with unchanged electrophysical properties throughout the entire volume. However, when it is subjected to certain physical or chemical influences, such as thermochemical modification, vibration hardening of the surface, or others, changes in microstructure occur throughout its entire near-surface layer. These changes are continuous along a certain zone of the material and provide significant useful information about mechanical deformations of objects, redistribution of elastic stress concentration, quality of technological operations of surface hardening, etc. Thus, the determination of the profiles of electrophysical material properties provides new advanced capabilities for the effective implementation of technological processes of testing, monitoring, and diagnosing critical states of objects of various functions.

In this study, we consider a method for simultaneously establishing the profiles of EC and MP, which is carried out by measurements with a surface eddy current probe (ECP) with subsequent calculations using a surrogate optimization algorithm and reduced-dimensional neural network metamodels. Thus, the problem of reconstructing the EC and MP profiles based on direct measurements of signal amplitude and phase by a surface ECP is, from a mathematical point of view, a multi-parameter inverse ill-posed problem.

1.1. Overview of Methods for Determining Profiles of Electrophysical Properties of Materials

Among the methods used to determine material property profiles, the most common ones are the inversion method and the method based on optimization algorithms [1–3], which minimize the difference between the results of calculations based on the mathematical model of field-material interaction and the measurement. However, such well-known approaches and methods that involve the use of multi-frequency measurements [4–7], improved probe constructions [8–10], compensation techniques [11], and the phenomenon of invariance [12,13] are rarely used due to a number of disadvantages. Thus, the modification of ECP constructions by incorporating additional coils complicates them. However, it provides further information about the measured electrophysical parameters, thus resulting in an increase in computing resources for its processing. The method of multifrequency excitation of eddy currents is characterized by the same disadvantages. It should also be noted that information processing in both of these methods is performed at the measurement stage, and this is a point for their implementation. Measuring techniques using compensation and the phenomenon of invariance are also marked by a common disadvantage, namely, the inability to measure both profiles of material properties simultaneously.

Despite significant advantages of optimization techniques in solving inverse problems in various applications, as noted by researchers in their works [1–3], they are unable to solve the problem of finding the profiles of EC and MP due to their high resource consumption, since the optimization algorithm involves the repeated use of a complex mathematical model of a direct problem with a significant number of desired variables, reaching hundreds in the target function. The approach proposed by the authors in [14–16] with a combination of optimization algorithms and physical multifrequency measurements of the ECP is rather difficult to implement. It takes a lot of effort to implement tool measurement with a complex schematic solution at swept-frequencies, proposed in [17–19]. The data-driven methods noted in [20] have a low accuracy of reconstructing the EC profiles. The procedure for reconstructing exclusively the distribution of ECs proposed in [21], which combines iterative inversion and finite element modeling, is computationally intensive.

Given the significant advantages of optimization algorithms and the ability to minimize the high resource intensity of target functions with surrogate optimization techniques [22–26], this method of reconstructing material property profiles has advantages for any arbitrary form of test objects. Moreover, supposing the surrogate model is created on the basis of neural networks and is a carrier of previously accumulated information on TO [27], it provides much more information about the measurement test process.

It is necessary to note the possibility of using both local [14,28] and global optimization methods [2,3,29] for this task, detailing optimization techniques. The application of the modified Newton–Raphson local search method, presented in [28] and improved for solving incorrectly stated and ill-posed problems using regularization and an unmodified sensitivity matrix, provides an acceptable calculation accuracy. However, the use of global optimization search methods [30], to find the minimum of a complex target function in a multidimensional space without special requirements for the points of initial approximation is more promising for this purpose. The most famous representatives of this class of algorithms are the stochastic evolutionary genetic algorithm GA and algorithms based on metaheuristics. Since the number of variables to be searched, i.e., the dimensionality of the factor space, is significant for profile recon reconstruction problems, the use of optimization algorithms is problematic due to the "curse of dimensionality".

Therefore, taking the above-mentioned into account, it is advisable to apply improved approaches based on modern effective optimization techniques, in particular, surrogate modeling techniques using reduced-dimensional metamodels, to determine the distributions of material properties. It is a key to a simultaneous solution of both the problem of calculating resource-intensive target functions and reducing the number of variables in optimization algorithms, which significantly decreases the error of solving the problem.

1.2. Overview of Search Space Reduction Methods

A number of recent studies on the simultaneous solution of both of these problems are aimed at using search algorithms for optimization in a low-dimensional compact space, which allows the dimensionality of the problem to be reduced by choosing a combination of variables or the main directions of the new basis, in which the bulk of the variation in the data of the full factor space is concentrated [31]. Reducing the cumbersomeness of high-dimensional surrogate models, significantly mitigating the effect of the "curse of dimensionality" in optimization algorithms is provided by Dimensionality Reduction Techniques (DRTs). In addition to these advantages, surrogate models, due to their approximation nature, also have the ability to accumulate a priori information about the TO obtained at the stage of their creation.

An experimental study of certain DRTs was performed and its results were published in [32], where the methods of Principal Component Analysis (PCA), Kernel Principal Component Analysis (KPCA), Autoencoders (AEs), and Variational Autoencoders (VAEs) were considered. The results demonstrated the advantage of AEs and the PCA method primarily by the criterion of modeling accuracy. However, the use of AEs causes significant difficulties in performing the inverse transformation after optimization when returning to the original factor space.

Articles [33,34] discussed the possibility of using the Uniform Manifold Approximation and Projection (UMAP) algorithm and its variants as a type of DRT performing a nonlinear reduction in the dimensionality of the search space. It should be noted that the inverse transformation of the obtained optimal solution from a low-dimensional space to the original high-dimensional space after applying the UMAP dimensionality reduction method is complex and almost always approximate. Unlike linear dimensionality reduction methods, such as PCA, UMAP applies nonlinear transformations, which makes it not always possible to accurately recover the desired variables in high-dimensional space. Therefore, taking into account all the advantages and disadvantages of the known DRTs, PCA seems to be promising for overcoming the problems of high dimensionality in the context of using surrogate optimization to determine the profiles of material properties of the TO.

Thus, the object of the study of this publication is the process of simultaneous determination of the profiles of material properties of the test objects by the eddy current method.

The subject of the study is the method of simultaneous determination of subsurface profiles of electrophysical parameters of metal objects by the eddy current method with a priori accumulation of information in surrogate models of reduced dimensionality.

The aim of this research is to study the effectiveness of the proposed method of joint simultaneous determination of electrical conductivity and magnetic permeability profiles in the subsurface zone of planar test objects using surrogate optimization techniques in the reduced dimension PCA-space and accumulation of a priori information in the surrogate model about all the main factors that form the signal of the surface eddy-current probe when varying the dimension of the compact space.

The article is structured as follows: introduction, three chapters, and conclusions. The introduction focuses on the relevance of the problem under study, analyzes modern methods for determining the profiles of electrophysical properties of materials and methods for reducing the dimensionality of the search space, and states the object, subject, and purpose of the research. The second section describes the main methodological aspects of the research and presents a surrogate optimization formulation of the inverse measurement problem. The third section presents the results of numerical experiments with the analysis of their accuracy. The conclusions include the discussion of the research results and the analysis of their effectiveness. Thus, determining the efficiency of the method of simultaneous identification of the electrophysical properties of materials in reduced dimensional spaces using eddy current measurements is the main contribution of the present study.

The innovation of the article lies in the study of the conditions for achieving a reasonable compromise between the accuracy of determining the near-surface distributions of the electrophysical material properties and the dimensionality of PCA-reduced order surrogate models, which determines, in turn, the accuracy of approximation of the electrodynamic model and the accuracy of finding the global optimum, and which are used in the method of simultaneous identification of profiles proposed by the authors with the accumulation of a priori information in neural network proxy models about the factors influencing the surface ECP signal.

2. Materials and Methods

In the modeling, we assume that the TOs have infinite geometric dimensions, and the TO medium is supposed to be linear, homogeneous, and isotropic. The determination of the EC and MP profiles is performed by numerical calculations based on the ECP measurement data. The algorithm for solving the inverse measurement problem involves the use of an electrodynamic model of the eddy-current testing process. To simplify it, the subsurface TO zone with certain structural differences caused, for example, by technological operations of surface hardening, is considered as conditionally multilayer. Each conditional layer is characterized by different constant values of material properties. The simulation of the continuity of the EC and MP profiles is ensured by a large number of conditional layers. The electromagnetic field is excited by the ECP excitation coil with a sinusoidal current I varying with a certain angular frequency ω. The model takes into account that this coil has a rectangular cross-section of finite dimensions, is characterized by a uniform current density across the cross-section and a certain number of turns W. Under these assumptions, the Uzal-Cheng-Dodd-Deeds [35–38] electrodynamic model of the eddy current test process was built in an analytical form modified by Theodoulidis [21].

The magnetic vector potential A in the thickness of the material TO is considered first for the case of excitation by a point source in the regions of the subsurface layer, which are given by L conditional layers, in particular, $0 < z < -d_1$ for the first layer; $-d_{\mathrm{t}-1} < z < -d_{\mathrm{t}}$ for the t-th layer; $-d_{\mathrm{t}} < z < -d_{\mathrm{t}+1}$ for the t+1-th layer; $-d_{\mathrm{t}+1} < z < -d_{\mathrm{L}-1}$ for the L-th layer. In this case, the thickness of the material of the TO is infinite, that is, $-d_{\mathrm{L}-1} < z < \infty$. The surface of the TO is taken as the origin of the regions in the cylindrical coordinate system (Figure 1).

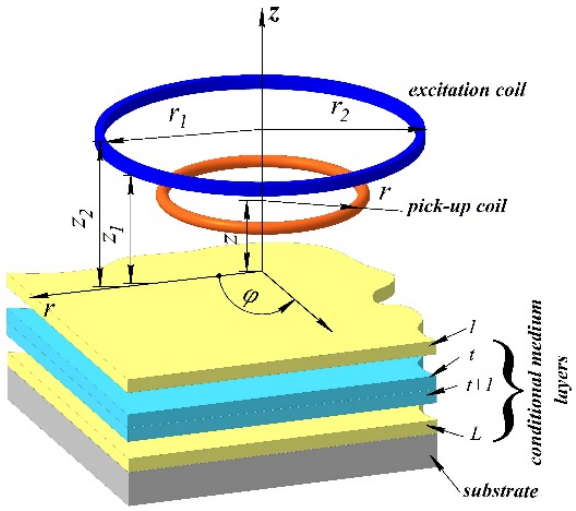

Figure 1. Geometric model of the profile measuring task.

In all these areas, the magnetic vector potential A is described by the Helmholtz partial differential equation:

$$\frac{\partial^2 A}{\partial r^2} + \frac{1}{r} \cdot \frac{\partial A}{\partial r} - \frac{A}{r^2} + \frac{\partial^2 A}{\partial z^2} = \widetilde{k}^2 \cdot A - \mu_0 \cdot I \cdot \delta(r - r_0) \cdot \delta(z - z_0), \tag{1}$$

where $\widetilde{k}^2 = j \cdot \omega \cdot \mu_r \cdot \mu_0 \cdot \sigma; j = \sqrt{-1}$;

δ is the Dirac delta function; r_0, z_0 are the coordinates of the location of the point source of the electromagnetic field; $\mu_0 = 4 \cdot \pi \cdot 10^{-7}$ H/m is the magnetic constant in vacuum; μ_r is relative magnetic permeability of the material; σ is the electrical conductivity of the material, S/m.

The general solution of Equation (1) is as follows:

$$A(r,z) = \int_0^\infty [A(\kappa) \cdot J_1(\kappa r) + B(\kappa) \cdot Y_1(\kappa r)] \cdot [C(\kappa) \cdot e^{\lambda z} + D(\kappa) \cdot e^{-\lambda z}] d\kappa, \tag{2}$$

where $\lambda = \sqrt{\kappa^2 + \widetilde{k}^2}$; $J_1()$, $Y_1()$ is the first-order Bessel functions of the first kinds.

In turn, the unknown coefficients in (2) are determined from the system of equations written for each media interface based on the fulfillment of the boundary conditions for the vector potential:

$$\begin{bmatrix} A_0 = A_1 \\ \frac{\partial A_0}{\partial z} = \frac{1}{\mu_{r1}} \cdot \frac{\partial A_1}{\partial z} \end{bmatrix}_{z=0} \quad and \quad \begin{bmatrix} A_{t+1} = A_t \\ \frac{1}{\mu_{t+1}} \cdot \frac{\partial A_{t+1}}{\partial z} = \frac{1}{\mu_t} \cdot \frac{\partial A_t}{\partial z} \end{bmatrix}_{z=-d_t} \tag{3}$$

In this case, an electromagnetic field is formed in the air environment in the area below the probe excitation coil as a superposition of its two components. The first component is the field of the coil in free space without a conductor $A^{(s)}$, and the second one is the field created by the eddy currents induced in the TO $A^{(ec)}$.

Finally, the magnetic vector potential of the subsurface ECP, taking into account the cross-section of the excitation coil, is as follows:

$$A(r_\delta, z_\delta) = A^{(s)} + A^{(ec)} = \int_0^\infty J_1(\kappa r_\delta) \cdot [C_s \cdot e^{\kappa z_\delta} + D_{ec} \cdot e^{-\kappa z_\delta}] d\kappa, \quad (4)$$

where:

$$C_s = \frac{\mu_0 \cdot i_0}{2} \cdot \frac{\chi(\kappa r_1, \kappa r_2)}{\kappa^3} \cdot (e^{-\kappa z_1} - e^{-\kappa z_2});$$
$$D_{ec} = \frac{(\kappa \cdot \mu_{t+1} - \lambda_1) \cdot V_{11}(1) + (\kappa \cdot \mu_{t+1} + \lambda_1) \cdot V_{21}(1)}{(\kappa \cdot \mu_{t+1} + \lambda_1) \cdot V_{11}(1) + (\kappa \cdot \mu_{t+1} - \lambda_1) \cdot V_{21}(1)} \cdot C_s;$$
$$i_0 = W \cdot I(r_2 - r_1)^{-1} \cdot (z_2 - z_1)^{-1};$$
$$\chi(x_1, x_2) = \left\{ x_1 \cdot J_0(x_1) - 2 \cdot \sum_{m=0}^{\infty} J_{2m+1}(x_1) \right\} - \left\{ x_2 \cdot J_0(x_2) - 2 \cdot \sum_{m=0}^{\infty} J_{2m+1}(x_2) \right\};$$
$$V(1) = T(1,2) \cdot T(2,3) \cdots T(L-2, L-1) \cdot T(L-1, L);$$
$$T_{11}(t, t+1) = \frac{1}{2} \cdot e^{(-\lambda_{t+1} + \lambda_t) dt} \cdot \left(1 + \frac{\mu_t}{\mu_{t+1}} \cdot \frac{\lambda_{t+1}}{\lambda_t}\right);$$
$$T_{12}(t, t+1) = \frac{1}{2} \cdot e^{(\lambda_{t+1} + \lambda_t) dt} \cdot \left(1 - \frac{\mu_t}{\mu_{t+1}} \cdot \frac{\lambda_{t+1}}{\lambda_t}\right);$$
$$T_{21}(t, t+1) = \frac{1}{2} \cdot e^{(-\lambda_{t+1} - \lambda_t) dt} \cdot \left(1 - \frac{\mu_t}{\mu_{t+1}} \cdot \frac{\lambda_{t+1}}{\lambda_t}\right);1$$
$$T_{22}(t, t+1) = \frac{1}{2} \cdot e^{(\lambda_{t+1} - \lambda_t) dt} \cdot \left(1 + \frac{\mu_t}{\mu_{t+1}} \cdot \frac{\lambda_{t+1}}{\lambda_t}\right);$$
$$\lambda_t = (\kappa^2 + j \cdot \omega \cdot \mu_0 \cdot \mu_t \cdot \sigma_t)^{\frac{1}{2}};$$

$A(r_\delta, z_\delta)$ is the azimuthal component of the vector potential, Wb/m; $\mathbf{V}(1)$ is a matrix with elements V_{11}, V_{21}; $\mathbf{T}()$ is a matrix with elements $T_{11}()$, $T_{12}()$, $T_{21}()$, $T_{22}()$; $\mu_0 = 4 \cdot \pi \cdot 10^{-7}$ is the magnetic constant in vacuum, H/m; μ_t, σ_t are the relative magnetic permeability and electrical conductivity of the conditional layer t, respectively; $J_m()$ are cylindrical Bessel functions of the first kind of m-order; r_δ, z_δ are the coordinates of the observation point P on the contour of the pick-up coil Lc in the cylindrical coordinate system, m; (r_2–r_1) is the width of the cross-section of the ECP excitation coil, m; (z_2–z_1) is the height of the cross-section of the ECP excitation coil, m; i_0 is the current density across the cross-section of the ECP excitation coil, A/m^2.

Thus, an output signal is generated in the pick-up coil of the ECP, which is calculated by the formula:

$$e_{\text{mod}} = -j \cdot \omega \cdot w_{\text{mes}} \cdot \oint_{Lc} A(r_\delta, z_\delta) dl_p = -j \cdot \omega \cdot w_{\text{mes}} \cdot 2 \cdot \pi \cdot r_\delta \cdot A(r_\delta, z_\delta), \quad (5)$$

where w_{mes} is the number of turns of the pick-up coil.

Based on the electrodynamic Model (5), the authors created and thoroughly tested a software product capable of calculating the output signal of a surface ECP under various measurement conditions. The verification of this product was carried out by comparing the results with both calculations based on analytical models obtained for one- and two-layer TOs [39] and numerical calculations by the finite element method in the COMSOL Multiphysics environment (AC/DC module) for a three-layer object [40], where the maximum relative error of amplitude and phase in determining the vector potential did not exceed 0.3% and 0.5%, respectively. Figure 2 shows a graphical illustration of the distributions of relative errors in calculating the amplitude and phase of the magnetic vector potential in the ECP measurement zone.

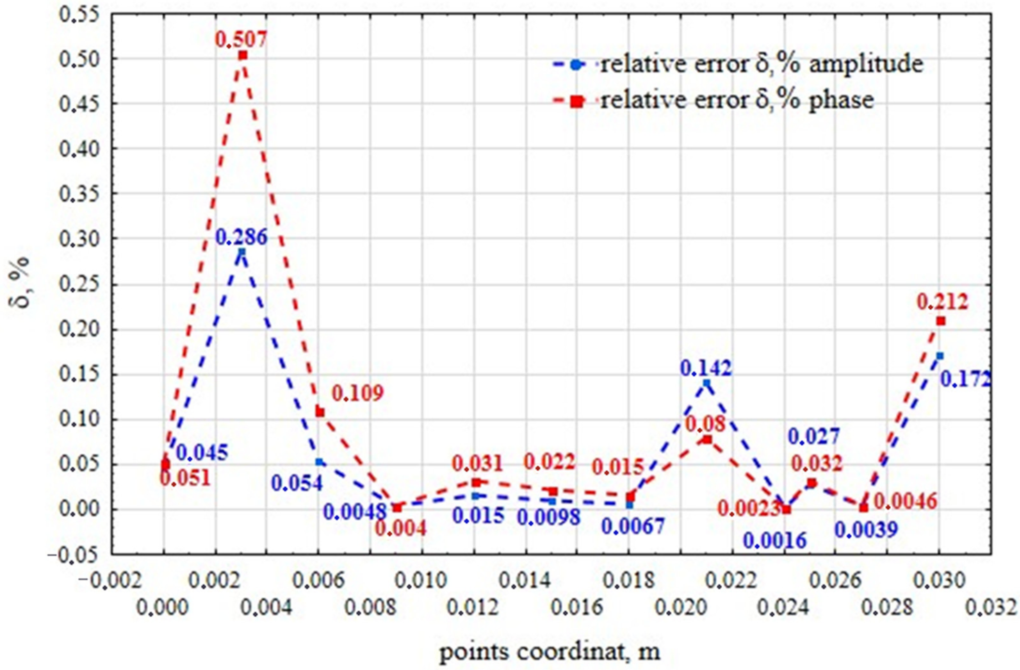

Figure 2. Distributions of relative errors in calculating the amplitude and phase of the magnetic vector potential.

Insignificant differences in calculations for electromagnetic computations are caused by errors inherent in each method. In particular, the analytical calculation is characterized by errors of truncation of the upper bound of the non-proprietary integral of the first kind, errors of approximate calculation of special Bessel functions and integrals of them, and error of the quadrature formula for calculating the non-proprietary integral. For the finite element method, the main errors are discretization ones and the dependence of the calculation results on the mesh construction, errors of shape functions of a given type, errors in solving systems of equations, etc.

It was believed that during the procedure of measuring the ECP over a planar object, the signal amplitude and phase are fixed in accordance with one of the classical schemes. The mathematically measured complex-valued signal e_{mes} can be represented in an algebraic form as the following expression: $e_{\text{mes}} = C_{\text{mes}} + j \cdot D_{\text{mes}}$, where C_{mes} and D_{mes} are its real and imaginary parts, respectively. Such a mathematical form of signal representation allows for more efficient construction of the target function F, which is used to determine the optimal values of the desired profile parameters.

In the mathematical form, the optimization problem is formulated as finding the minimum of a functional on the domain R^n: $F* = \underset{\sigma,\mu}{\text{argmin}}\{F(\boldsymbol{\sigma}, \boldsymbol{\mu}, f, z) : \ \boldsymbol{\sigma}, \boldsymbol{\mu} \in R^n\}$, $n = 2 \cdot L + 2$, where R^n is an n-dimensional Euclidean space, i.e., a domain of vectors $(\sigma_1, \ldots, \sigma_L, \mu_1, \ldots, \mu_L)^T$, all components of which are real values.

Then the task of identifying EC and MP profiles is minimized to the following quadratic function:

$$F(\boldsymbol{\sigma}, \boldsymbol{\mu}, f, z) = (C_{\text{mes}} - G_{\text{metamod}}(\boldsymbol{\sigma}, \boldsymbol{\mu}, f, z))^2 + (D_{\text{mes}} - Z_{\text{metamod}}(\boldsymbol{\sigma}, \boldsymbol{\mu}, f, z))^2 \to \text{min}in \tag{6}$$

where: $e_{\text{metamod}} = G_{\text{metamod}} + j \cdot Z_{\text{metamod}}$ is the value of the ECP signal obtained using a surrogate model (metamodel, i.e., a model for an electrodynamic model); σ, μ are the corresponding vectors of material properties of the TO determining the desired profiles; f is the frequency of the excitation field; z is the lift-off. Then the desired parameters in the optimization algorithm are the components of the EC and MP vectors, the numbers of which determine the value of the right-hand side of the target Function (6) $G_{\text{metamod}}(\boldsymbol{\sigma}, \boldsymbol{\mu}, f, z)$ and $Z_{\text{metamod}}(\boldsymbol{\sigma}, \boldsymbol{\mu}, f, z)$.

The modeling was based on the research methodology, which is discussed in detail by the authors and illustrated by examples in [22–25,27] and involves the following main steps "exact" solution of the direct electrodynamic problem of interaction of the quasi-stationary electromagnetic field generated by the surface ECP with a conductive planar TO with piecewise constant profiles of material properties and calculation of the ECP signal; designing computational experiments [41] and building proxy models (metamodels) based on deep fully connected MLP-neural networks with a priori information about the TO; solving the inverse problem of determining profiles by an optimization population metaheuristic algorithm for finding a global extremum using a surrogate model. The general scheme of the proposed method is illustrated in Figure 3.

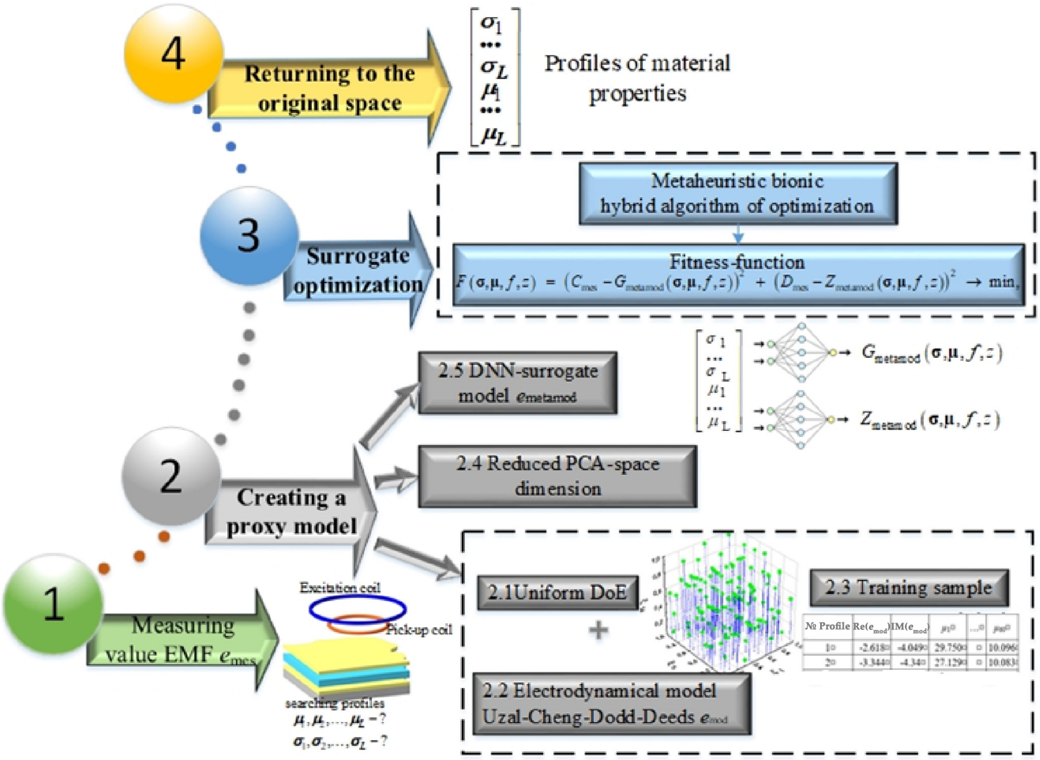

Figure 3. General scheme of the method for determining material property profiles.

In this research, the final stage has certain peculiarities. The design of computational experiments includes all the main factors determining the formation of the output signal of the surface ECP, in particular, the material properties of the TO, the frequency of the electromagnetic field of sensing, and the lift-off [42]. This allows of accumulating additional information about the TO at the stage preceding the optimization solution, using the unique generalizing capabilities of deep neural networks used to create a surrogate model. Surrogate optimization is performed not in the full design space, the dimension of which is determined by the double number of conditional layers of the subsurface zone of the TO, but in a reduced space of reduced dimensionality, which retains almost all the properties of the full space with a slight loss of information. Such a compact representation of the search space was made possible by using the PCA method. The aim of PCA is to find a space that represents the direction of maximum variance of the data in the design of experiment (DOE) matrix. The PCA-space is defined by the addition of orthogonal principal components, i.e., vectors. The principal components are calculated using the SVD-decomposition of the Gram matrix by singular values. In this case, the left and right singular matrices constitute orthonormal bases that correspond to the sorted eigenvalues associated with the singular numbers of the matrix. The selected part of the left singular matrix is used as eigenvectors to construct the PCA-space. The dimensionality of this space can be adjusted by selecting a larger or smaller part of the eigenvectors, taking into account the values of the corresponding eigenvalues of the matrix.

Thus, when performing optimization, a compromise can be found between the computational complexity of the problem and the accuracy of its solution by testing and choosing the dimension of the reduced search space. After applying the optimization algorithm, the back-projection is performed to return to the original design space to determine the desired EC and MP profiles.

3. Results

One of the stages of the proposed methodology is the creation of a computerized homogeneous DOE on Sobol's quasi-sequences, which has low discrepancy rates both for the volumetric case and for two-dimensional projections. This is necessary for the construction of surrogate models. The task of reconstructing the EC and MP profiles is carried out using a metamodel with consideration of the four factors $\boldsymbol{\sigma}$, $\boldsymbol{\mu}$, and f, z, which are the most influential in eddy-current measurements by surface ECP. Then, the implementation of a multidimensional homogeneous quasi-design is performed on the following combinations of Sobol's LP_{τ}-sequences ξ_1, ξ_6, ξ_{14}, ξ_{17} [41]. The numerical values of the coordinates of the points of such a DOE N_{profile} = 8191 with improved two-dimensional projections on a unit scale are shown in Table 1.

Table 1. Design of experiment on Sobol's quasi-sequences in unit hyperspace.

Number of the Sequence	Number of the DOE Point								
	1	**2**	...	**4000**	**4001**	**4002**	**4003**	**4004**	...
ξ_1	0.5	0.25	...	0.023193	0.523193	0.273193	0.773193	0.148193	...
ξ_6	0.5	0.75	...	0.318115	0.818115	0.568115	0.068115	0.443115	...
ξ_{14}	0.5	0.75	...	0.08374	0.58374	0.83374	0.33374	0.20874	...
ξ_{17}	0.5	0.25	...	0.631104	0.131104	0.881104	0.381104	0.256104	...
Number of the Sequence	**Number of the DOE Point**								
	...	**6500**	**6501**	**6502**	...	**8189**	**8190**	**8191**	
ξ_1	...	0.150757	0.650757	0.400757	...	0.749878	0.499878	0.999878	
ξ_6	...	0.847046	0.347046	0.097046	...	0.879761	0.629761	0.129761	
ξ_{14}	...	0.198608	0.698608	0.948608	...	0.997925	0.747925	0.247925	
ξ_{17}	...	0.341187	0.841187	0.091187	...	0.634644	0.384644	0.884644	

The transition from the unit hyperspace to the real factor space was made by scaling. It is taken into account that the change in the microstructure in the subsurface zone of the TO is characterized by the initial values of the EC σ_{deep} and the MP μ_{deep}, which remain unchanged at a certain depth of the subsurface zone, and the influence of any of the physical factors (temperature, strain, etc.) on the TO leads to the fact that the values of the EC and MP, i.e., σ_{surf} and μ_{surf}, change as much as possible on their surface. We will assume that the profiles of material properties vary within ±15% relative to the values of EC and MP on the surface of the TO. It is within these limits, which can be adjusted if necessary, that the profiles are reconstructed. The EC profile is characterized by the values $\sigma_{\mathrm{deep}} = 2\cdot10^6$ S/m, $\sigma_{\mathrm{surf}} = 9.2\cdot10^6$ S/m, and the MP profile is characterized by $\mu_{\mathrm{deep}} = 10$, $\mu_{\mathrm{surf}} = 29.78$ (Table 2, point 1). Then, taking into account the specified limits, the ranges of change in the EC parameters on the surface of the TO will be $7.82 \cdot 10^6 \leq \sigma_{surf} \leq 10.1 \cdot 10^6$ S/m, and the MP will be $24.531 \leq \mu_{surf} \leq 35.028$ [25].

Table 2. Total training sample of size 8191 × 122 for creating metamodels.

№ Profile	Re(e_{mod})	Im(e_{mod})	μ_1	...	μ_{60}	σ_1, S/m	...	σ_{60}, S/m	f, kHz	$z \cdot 10^{-3}$, m
1	−2.618	−4.049	29.750	...	10.096	8,834,221	...	2,073,403	10.5	1.5
2	−3.344	−4.34	27.129	...	10.083	9,490,569	...	2,107,756	15.25	1
3	−1.651	−3.074	32.371	...	10.109	8,177,872	...	2,039,050	5.75	2
4	−1.082	−2.156	25.819	...	10.077	7,849,698	...	2,021,873	3.375	2.25
5	−3.021	−4.392	31.061	...	10.102	9,162,395	...	2,090,580	12.875	1.25
...	...	...	...	...	...	...	...	...	...	...
4000	−0.588	−1.372	32.123	...	10.107	8,233,531	...	2,041,963	1.7	2.106
4001	−1.976	−2.886	29.502	...	10.095	7,577,287	...	2,007,615	6.451	0.6059
4002	−3.438	−5.526	34.744	...	10.120	8,889,879	...	2,076,316	15.951	1.606
4003	−0.903	−1.749	24.751	...	10.071	8,356,662	...	2,048,408	2.591	1.7622
...	...	...	...	...	...	...	...	...	...	...
6500	−2.007	−3.224	32.642	...	10.110	9,417,058	...	2,103,909	7.148	1.4324
6501	−1.534	−2.355	26.089	...	10.078	9,745,232	...	2,121,085	4.773	1.1824
6502	−3.093	−5.503	31.331	...	10.103	8,432,536	...	2,052,379	14.273	2.1824
...	...	...	...	...	...	...	...	...	...	...
8188	−2.721	−3.575	27.128	...	10.083	8,518,648	...	2,056,886	10.4601	0.7692
8189	−3.82	−6.145	32.370	...	10.109	9,831,345	...	2,125,592	19.9601	1.7692
8190	−3.338	−4.77	29.749	...	10.096	9,174,997	...	2,091,239	15.2101	1.2692
8191	−1.602	−3.195	34.991	...	10.121	7,862,300	...	2,022,533	5.7101	2.2692

For example, the model piecewise steady-state representation of profiles is carried out according to the law of distribution of the "exponent" for the EC and the "gaussian" for the MP, referring to the typical dependencies determined experimentally in [38] for various technological operations. Within the specified boundary limits of changes in the material properties of the TO in the real design space, we calculated the distributions of EC and MP for all points of the DOE, which corresponds to the number of profiles in the total sample $N_{profile}$ with a sampling of the subsurface zone $D = 3 \cdot 10^{-4}$ m by $L = 60$ conditional layers. Table 2 shows the numerical values of the material properties μ_{surf}, σ_{surf} on the surface of the TO and at the depth of the subsurface zone μ_{deep}, σ_{deep} at the DOE points in real hyperspace. In addition, the creation of the DOE requires setting the frequency of the electromagnetic excitation field, which is determined by the range of $1 \leq f \leq 20$ kHz and is informative for observing the response of the probe signal at different sensing depths of the TO and the lift-off, which varies in the range of $0.5 \leq z \leq 2.5$ mm.

Using the electrodynamic Model (5), we calculated the output signals of the ECP, taking into account the most influential factors, the results of which are shown in Table 2.

To visualize the presentation of sample profiles of the training sample, let us illustrate them with graphs for some of their cases (Figures 4 and 5).

In the full factor space, we obtained a dataset of size $N_{profile} \times (2L + 2)$. For this case, the dimension of the factor space is quite significant, as it is 122. Therefore, building a metamodel in such a space is cumbersome. This created sample is used for the next stage of the research, namely, the transition to the reduced dimensionality space using the PCA method based on the SVD-decomposition of the Gram matrix, which makes it possible to obtain the data matrix **G** obtained by projection.

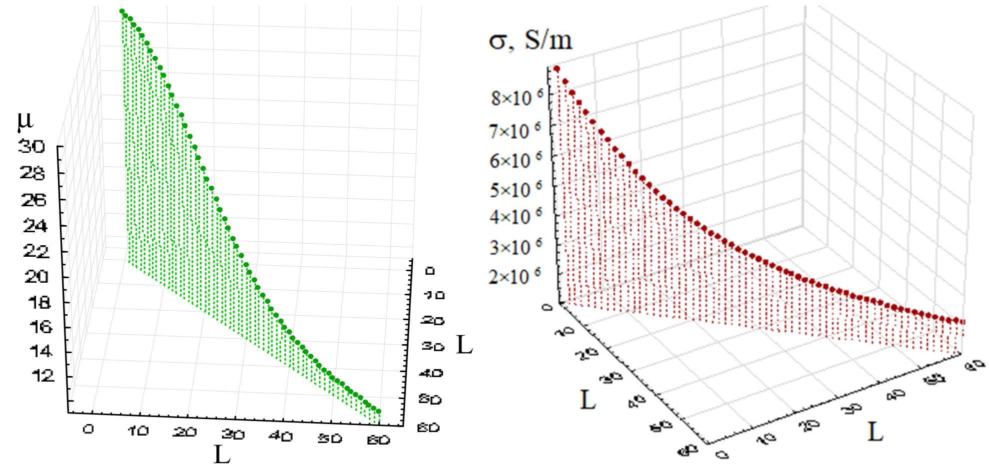

Figure 4. Plots of MP and EC profiles of the training sample for the first sample.

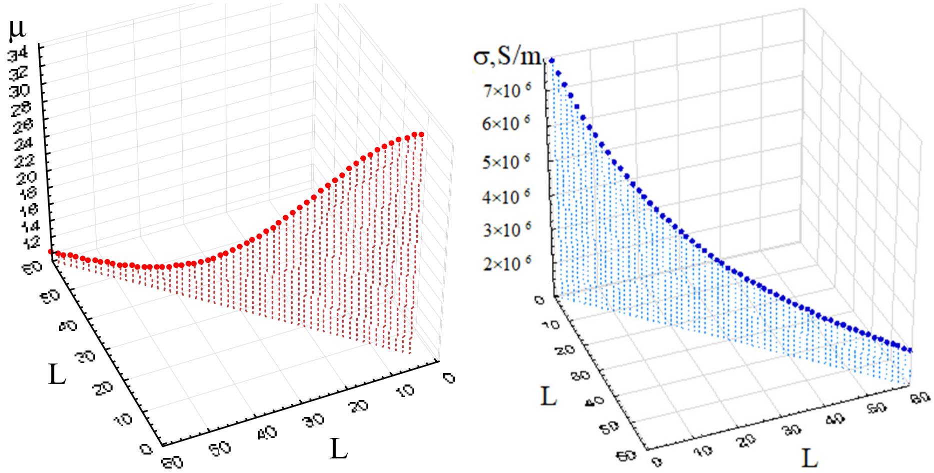

Figure 5. Plots of MP and EC profiles of the training sample for the second sample.

Thus, to determine the effectiveness of the proposed optimization method for reconstructing profiles in PCA-space in terms of accuracy, we varied its dimension based on the values of the eigenvalues of the Gramm's matrix. Neural network surrogate models were created in PCA-space. For all cases of deep learning of neural networks, the matrix **G** in the reduced space has the size $N_{\text{profile}} \times n_{\text{red}}$, where n_{red} is the number of basis vectors **g** in the new space, which, in the experiments, were taken to be 51, 55, 62, 63, 66, 70. For example, Tables 3 and 4 show the matrices **G** for $n_{\text{red}} = 66$ and $n_{\text{red}} = 70$, respectively. The number of profiles in the training sample was distributed in the following ratio: $N_{\text{traine}} = 4211$ for training, $N_{\text{test}} = 903$ for testing, and $N_{\text{CV}} = 903$ for cross-validation. However, later on, the profiles that did not participate in neural network training were used as synthesized profiles to verify the reliability of the solution to the inverse problem of profile reconstruction.

The metamodels were built using deep learning neural networks, for which the inputs are a matrix of **g**-parameters, and the outputs of each of the two networks are, respectively, the real and imaginary parts of the EMF of ECP. It should be noted that instead of a single complex-valued neural networks model, two truly significant ones were created, separately for each part of the EMF [23].

Table 3. Matrix **G** of size 8191 × 66 for creating a metamodel in reduced space.

№ Point	g_1	g_2	...	$g_{63} \cdot 10^{-3}$	$g_{64} \cdot 10^{-6}$	$g_{65} \cdot 10^{-5}$	$g_{66} \cdot 10^{-6}$
1	−34,344,006	−40,876.45	...	1.1182417	−4.3655575	−2.7324841	−9.9903449
2	−36,406,779	469,672.51	...	1.3578367	1.0050861	4.8739237	−9.5527309
3	−32,281,232	−551,426.58	...	−0.84519701	1.8541591	2.6137071	1.4317285
4	−31,249,845	−806,701.24	...	0.81916363	−3.4961978	2.5458931	-16.278854
5	−35,375,392	214,397.8	...	−0.72947157	1.8999668	2.4602704	7.8984196
...	...	...	...	...	...	...	...
4000	−32,456,154	−508,125.92	...	0.40719932	−4.3855376	1.4012109	−13.124172
4001	−30,393,713	−1,018,605.3	...	−0.3012072	0.92514422	0.69598148	12.750525
4002	−34,518,930	2411.1632	...	-0.04193999	−0.3775342	0.49929265	−2.8554507
4003	−32,843,130	−412,346.93	...	0.17409037	−0.21069551	−4.7533737	0.37582572
...	...	...	...	...	...	...	...
6500	−36,175,746	412,500.31	...	−1.9820983	−0.91582073	3.028646	17.003993
6501	−37,207,131	667,781.07	...	−0.22798476	−1.4959489	−1.3101498	8.1150943
6502	−33,081,590	−353,341.45	...	−1.5273564	0.10773142	1.2167706	8.5331139
...	...	...	...	...	...	...	...
8188	−33,352,224	−286,351.94	...	−0.50085944	1.2109117	6.7995709	8.1435655
8189	−37,477,772	734,747.26	...	0.94150458	−2.7386983	1.5916526	−14.582567
8190	−35,414,998	224,197.78	...	−0.5216811	−2.8553455	0.63959491	8.9033673
8191	−31,289,451	−796,901.49	...	−0.94330238	−0.73879451	−2.1224067	2.6894707

Table 4. Matrix **G** of size 8191 × 70 for creating a metamodel in reduced space.

№ Point	g_1	g_2	...	$g_{67} \cdot 10^{-6}$	$g_{68} \cdot 10^{-6}$	$g_{69} \cdot 10^{-6}$	$g_{70} \cdot 10^{-6}$
1	−34,344,006	−40,876.45	...	−1.7857154	−2.6970985	1.3360738	8.9565972
2	−36,406,779	469,672.51	...	−1.8613386	−6.5017436	−2.0646505	−0.22363006
3	−32,281,232	−551,426.58	...	−0.99542366	−1.1564342	2.0872159	1.7184009
4	−31,249,845	−806,701.24	...	−6.4539495	−4.7595708	−2.1812924	4.3448066
5	−35,375,392	214,397.8	...	3.6382894	−0.26527532	1.0888234	2.6050557
...	...	...	...	...	...	...	...
4000	−32,456,154	−508,125.92	...	−5.7883783	0.50156034	2.4373703	-0.1625042
4001	−30,393,713	−1,018,605.3	...	1.471846	0.14645352	3.5148004	1.0478703
4002	−34,518,930	2411.1632	...	−0.54317705	1.7661484	−2.8734536	−1.2151284
4003	−32,843,130	−412,346.93	...	2.9292836	−0.26367515	−1.3622012	−3.8984309
...	...	...	...	...	...	...	...
6500	−36,175,746	412,500.31	...	0.03427952	2.2194627	1.2633268	1.9746877
6501	−37,207,131	667,781.07	...	2.3673397	2.3233701	6.2805614	3.1002567
6502	−33,081,590	−353,341.45	...	−2.1026837	3.2496936	−0.11656799	−1.1680763
...	...	...	...	...	...	...	...
8188	−33,352,224	−286,351.94	...	0.89647088	−0.43069366	0.23573517	0.83320714
8189	−37,477,772	734,747.26	...	−0.42935363	4.1352578	0.64174154	−1.1018135
8190	−35,414,998	224,197.78	...	0.23375807	1.2310493	3.6886197	2.8839691
8191	−31,289,451	−796,901.49	...	3.6561543	1.7678272	−1.8595518	0.27479352

To design neural networks, we made an approximate choice of their architecture with up to five hidden layers, a variable number of neurons in them, and one output. Various learning rules were applied, including Levenberg–Marquardt, Conjugate Gradient, Quickprop, Delta-Bar-Delta, etc. and activation functions such as sigmoid, tanh, RELU. The neural network variants were evaluated by RMSE (Root Mean Square Error), MAE (Mean Absolute Error), and R^2 (Coefficient of Determination). As a result, for this task, it turned out to be appropriate to choose an architecture with four hidden layers, a hyperbolic tangent activation function for each of them, and a Levenberg–Marquardt learning rule. The encoding of the general structure of the neural networks is presented in the form:

rMLP-n_1-n_2-n_3-n_4-1, where n_1, n_2, n_3, n_4 is the number of neurons in each hidden layer for the real part of the EMF and iMLP-n_1-n_2-n_3-n_4-1, respectively, for the imaginary part. This is the notation used in the tables. Since the inputs to the neural networks are samples of training data with a large difference in values (Tables 3 and 4), standardization was used to normalize the feed on the inputs of the neural network values comparable in size.

We obtained neural networks with four hidden layers for the real and imaginary parts of the EMF, respectively, taking into account a different number of basis vectors **g**, the training efficiency of which was evaluated by the values of the mean square errors MSE (Table 5). The efficiency of neural networks with the PCA-space dimension less than 63 is not sufficiently acceptable (MSE of the order of 10^{-4}), so for further analysis and construction of neural networks, only cases of dimensions 63, 66, 70 were selected, for which the MSE is much smaller than the specified one.

Table 5. Mean square error of the metamodels.

Eigenvalues of the Gram Matrix	Dimensionality PCA-Space	Mean Square Error MSE	
		$\mathrm{Re}(e_{metamod})$	$\mathrm{Im}(e_{metamod})$
433.166	51	$5.2 \cdot 10^{-4}$	$1.17 \cdot 10^{-3}$
359.081	55	$3 \cdot 10^{-4}$	$5.9 \cdot 10^{-4}$
24.699	62	$3.4 \cdot 10^{-4}$	$6.95 \cdot 10^{-4}$
0.057	63	$1.24 \cdot 10^{-6}$	$1.043 \cdot 10^{-6}$
$9.341 \cdot 10^{-8}$	66	$3.48 \cdot 10^{-7}$	$2.19 \cdot 10^{-6}$
$2.276 \cdot 10^{-8}$	70	$5.206 \cdot 10^{-7}$	$1.461 \cdot 10^{-6}$

As a result, for n_{red} = 66, we obtained the deep neural networks rMLP-16-17-15-11-1 and iMLP-16-17-16-13-1 with four hidden layers for the real and imaginary parts of the EMF, respectively. The validity of the obtained metamodels was evaluated by the errors $\mathrm{RMAE}_{metamod}$, % (Relative Mean Absolute Error) separately for the training, cross-validation, and test samples, the results of which are shown in Table 6, and by analyzing scatter plots (Figures 6 and 7) and residual histograms (Figures 8 and 9).

Table 6. Error of the approximation $\mathrm{RMAE}_{metamod}$, % of obtained metamodels for dimension 66 of PCA-space.

Metamodels	rMLP-16-17-15-11-1	iMLP-16-17-16-13-1
Training sample, N_{traine} = 4211	0.0232	0.0305
Cross-validation sample, N_{CV} = 903	0.0307	0.0389
Test sample, N_{test} = 903	0.0287	0.0395
The total sample for training, N = 6017	0.0251	0.0333

Neural networks of a similar architecture were obtained for n_{red} = 70—rMLP-16-17-16-14-1 and iMLP-16-16-15-12-1. The validity of these metamodels was evaluated as in the previous case using the same indicators: $\mathrm{RMAE}_{metamod}$, % (Table 7), scatter diagrams (Figures 10 and 11), histograms of residuals (Figures 12 and 13).

Table 7. Error of the approximation $\mathrm{RMAE}_{metamod}$, % of obtained metamodels for the dimensionality of 70 PCA-space.

Metamodels	rMLP-16-17-16-14-1	iMLP-16-16-15-12-1
Training sample, N_{traine} = 4211	0.0272	0.0262
Cross-validation sample, N_{CV} = 903	0.0352	0.0367
Test sample, N_{test} = 903	0.0369	0.0345
The total sample for training, N = 6017	0.0299	0.029

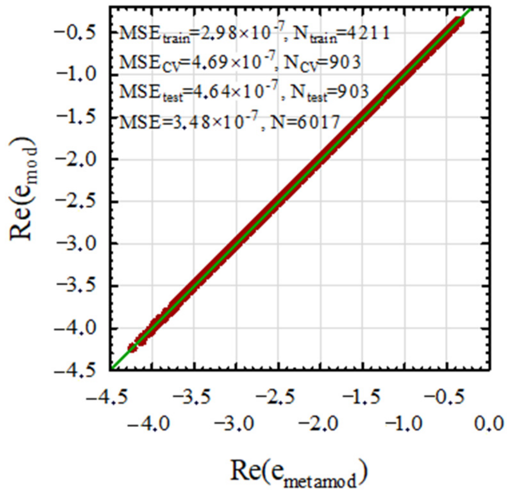

Figure 6. Statistical evaluation of the quality of metamodels n_{red} = 66. Scatter plot of the metamodel rMLP-16-17-15-11-1.

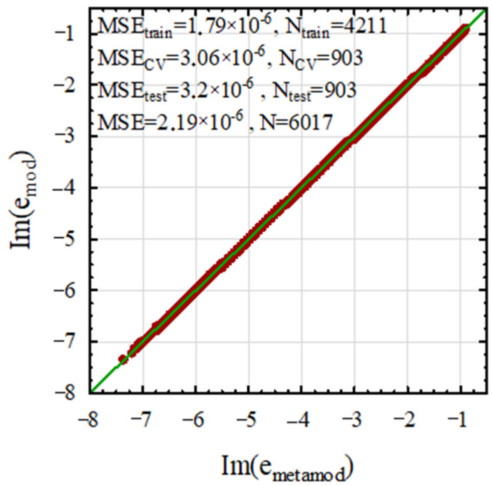

Figure 7. Statistical evaluation of the quality of metamodels n_{red} = 66. Scatter plot of the metamodel iMLP-16-17-16-13-1.

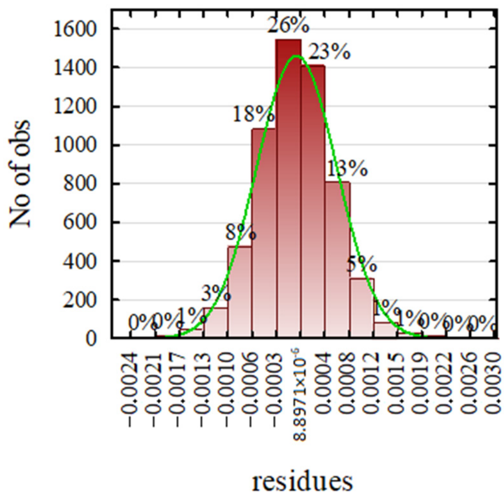

Figure 8. Statistical evaluation of the quality of metamodels n_{red} = 66. Histogram of residuals of the metamodel rMLP-16-17-15-11-1.

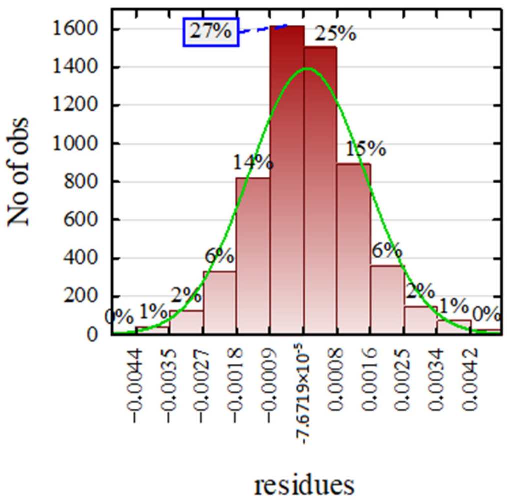

Figure 9. Statistical evaluation of the quality of metamodels n_{red} = 66. Histogram of residuals of the metamodel iMLP-16-17-16-13-1.

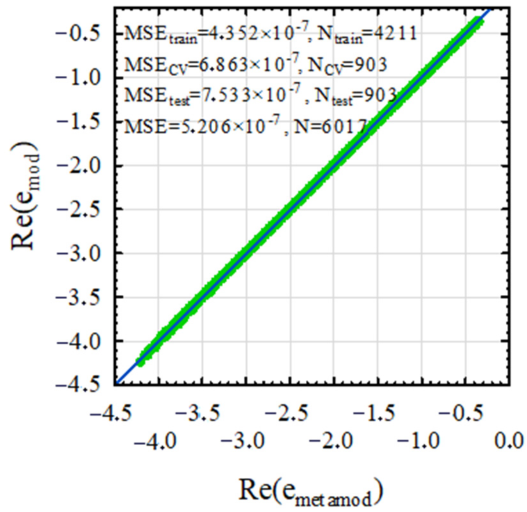

Figure 10. Statistical evaluation of the quality of metamodels for n_{red} = 70. Scatter plot of the metamodel rMLP-16-17-16-14-1.

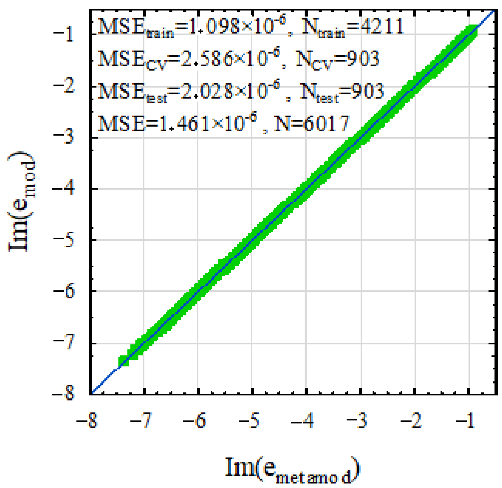

Figure 11. Statistical evaluation of the quality of metamodels for n_{red} = 70. Scatter plot of the metamodel iMLP-16-16-15-12-1.

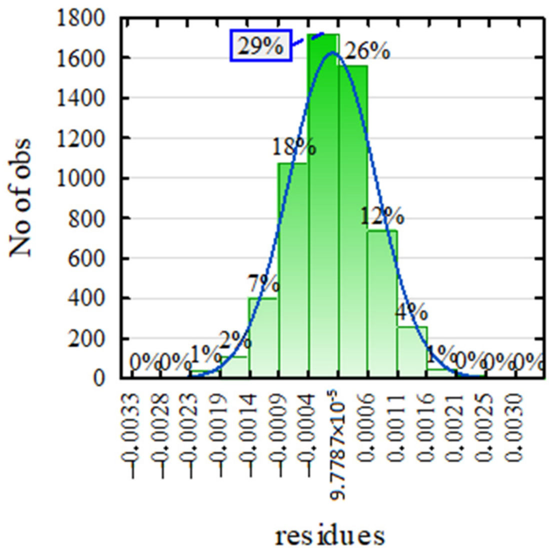

Figure 12. Statistical evaluation of the quality of metamodels for n_{red} = 70. Histogram of the residuals of the metamodel rMLP-16-17-16-14-1.

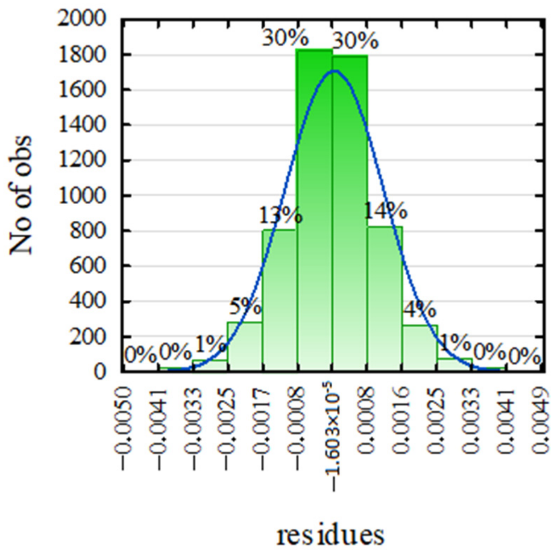

Figure 13. Statistical evaluation of the quality of metamodels for n_{red} = 70. Histogram of the residuals of the metamodel iMLP-16-16-15-12-1.

In addition, we tested the informativeness and adequacy of the created metamodels at the level of significance of 5% by the numerical indicators of the coefficient of determination and Fisher's F-ratio [43,44], the results of which are presented in Table 8.

Table 8. Checking the adequacy and informativeness of metamodels.

n_{red}	Metamodels	Statistical Parameters	Adequacy	Informativeness
66	rMLP-16-17-15-11-1	α = 5%, $v_D = 66$, $v_R = 5950$ $F^{table}_{0.05;66;5950} = 1.305$	$F^{total}_{66;5950} = 2.48 \cdot 10^8$	R^2= 0.9999; $F^{total}_{66;5950} = 3.26 \cdot 10^9$
	iMLP-16-17-16-13-1		$F^{total}_{66;5950} = 8.11 \cdot 10^7$	R^2= 0.999999; $F^{total}_{66;5950} = 7.01 \cdot 10^6$
70	rMLP-16-17-16-14-1	α = 5%, $v_D = 70$, $v_R = 5946$ $F^{table}_{0.05;70;5946} = 1.296$	$F^{total}_{70;5946} = 1.56 \cdot 10^8$	R^2= 0.99999; $F^{total}_{70;5946} = 2.45 \cdot 10^9$
	iMLP-16-16-15-12-1		$F^{total}_{70;5946} = 1.14 \cdot 10^8$	R^2= 0.999988; $F^{total}_{70;5946} = 7.09 \cdot 10^6$

All the created metamodels are adequate, since the calculated values of Fisher's criterion for them significantly exceed their critical values. The acceptable informativeness of the created metamodels is also indicated by the high coefficient of determination, which is significantly reliable according to Fisher's criterion at the level of 5%.

The inverse problem was solved using a metaheuristic stochastic global optimization algorithm [45,46]. For this purpose, a hybrid multi-agent particle swarm optimization algorithm with evolutionary formation of the swarm composition was used, the effectiveness of which was previously proven by the authors. Improving the accuracy of solutions in the study was achieved by using a multi-start technique. By a series of starts of the optimization algorithm, twenty-three solutions were obtained and inverse transformations were performed from the PCA-space of the principal components to the primary space, and the actual MP and EC profiles were found for two test measurements of the EMF at different space dimensions. Figure 14 shows examples of the obtained profiles for the PCA space dimension of 63.

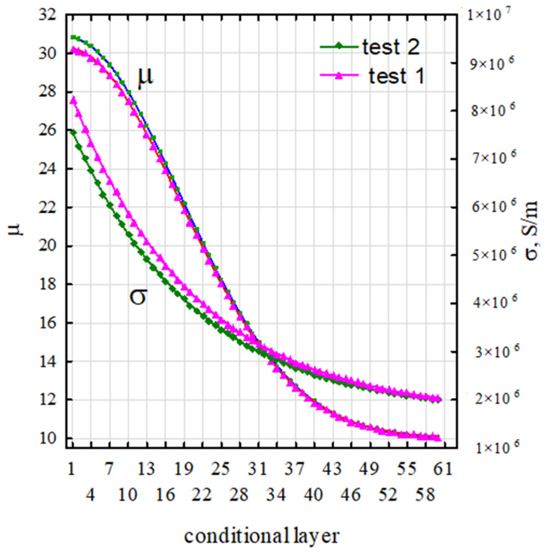

Figure 14. Examples of the obtained profiles for the PCA space dimension equal to 63.

The limits of the obtained errors in determining of the profiles RMAE, %, are given in Table 9, and the graphs of the distributions of the absolute error modules of the profiles for test 1, as an example, are shown in Figures 15 and 16.

Table 9. Ranges of change in reconstruction profile variants errors of RMAE.

Number of the Test Measurement	Results and Measurement Conditions	RMAE$_\mu$, %			RMAE$_\sigma$, %		
		n_{red} = 63	n_{red} = 66	n_{red} = 70	n_{red} = 63	n_{red} = 66	n_{red} = 70
Test 1	Re (e_{mes}) = −0.58 Im (e_{mes}) = −1.236 f = 1533.52 Hz z = 1.065 mm	0.324–8.483	0.27–5.579	0.042–4.884	0.17–4.824	0.22–2.062	0.137–3.14
Test 2	Re (e_{mes})= −2.557 Im (e_{mes}) = −3.827 f = 9599.4 Hz z = 1.0068 mm	0.208–4.933	0.341–4.135	0.278–3.643	0.602–5.105	0.177–2.166	0.197–3.093

Finally, we obtained the EC and MP profiles for each test measurement by the probe by averaging over the starts. Figures 17 and 18 show the error values RMAE, % of reconstructed profiles for these measurements, taking into account the different dimensions of the PCA-spaces.

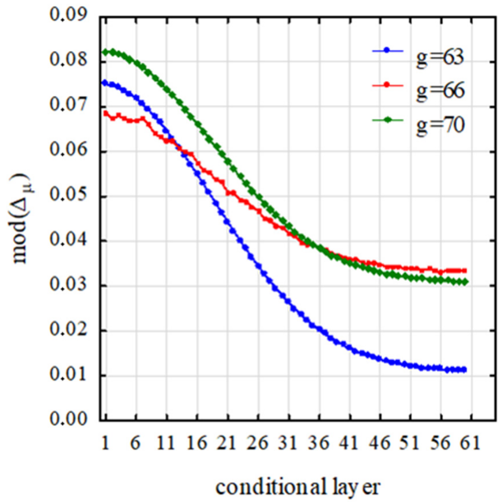

Figure 15. Distributions of absolute errors module of profile reconstruction for test measurement 1 of magnetic permeability.

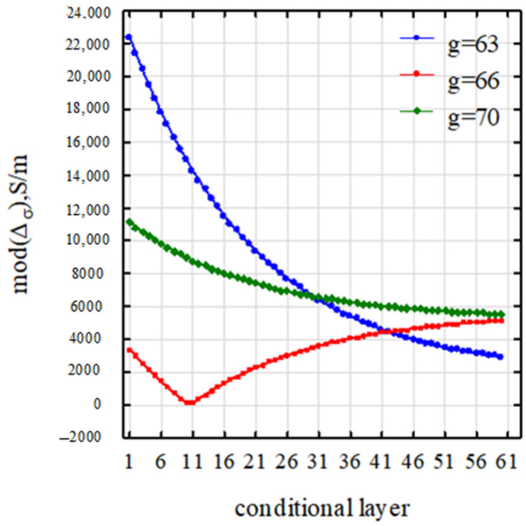

Figure 16. Distributions of absolute errors module of profile reconstruction for test measurement 1 of electrical conductivity.

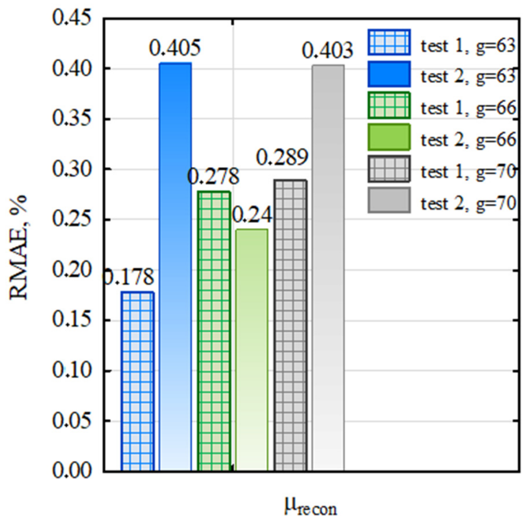

Figure 17. Errors in determining MP profiles RMAE,% for two test measurements at different dimensions of PCA-spaces.

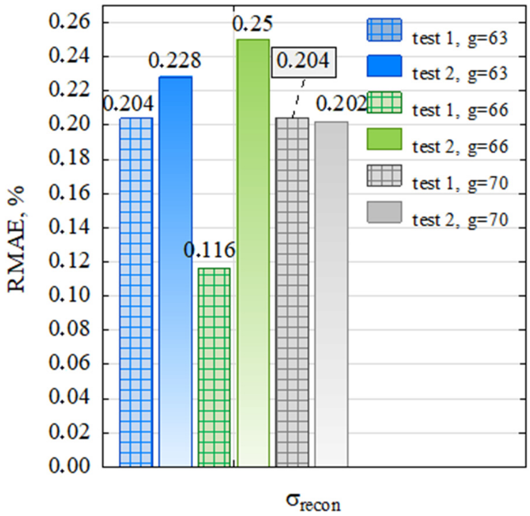

Figure 18. Errors in determining EC profiles RMAE,% for two test measurements at different dimensions of PCA-spaces.

Similar numerical experiments were conducted for other PCA-space dimensions, in particular 51, 55, 62, 63.

4. Discussions and Conclusions

Significant advantages of the PCA method compared to some other methods of reducing the dimensions of the design space are: the ability to extract the principal components that contain the largest part of the variance of the data in them; effectively reducing the dimensionality of the data while retaining a significant part of the information contained in the original data set; simple and efficient computational procedures performed by linear algebraic transformations; easy backward transformation to the original factor space after the optimization algorithm is executed in reduced space factors. Therefore, it is the most effective for overcoming high-dimensional problems, combined with the use of surrogate optimization techniques to determine the profiles of material characteristics of the TO.

Similar research in terms of methodology was previously conducted by the authors with the a priori consideration of a limited number of influential factors in the metamodels, namely, two factors—**μ** and **σ** [23], three—**μ**, **σ**, *f* [24]; four—**μ**, **σ**, *f*, *z* [25]. Numerical experiments were performed in all cases according to the same scheme. With the increase in the amount of a priori information about the TO, there was a tendency to improve the accuracy of the results of determining the profiles.

Therefore, to improve the accuracy of profile reconstruction, it is necessary to take into account information on all the most influential factors considerably influencing the formation of the surface ECP signal. This study took into account all the important factors as in [25]. In addition, the accuracy of solving the inverse problem of reconstructing the profiles of the MP and EC is affected by a number of components, one of which is the accuracy of the created metamodels. This study shows that, with an excessive reduction in the dimensionality of the PCA-space, which is a consequence of the exclusion of basis vectors corresponding to significant eigenvalues, the problem of constructing metamodels with satisfactory MSE performance arises. At the same time, when more information is taken into account in the metamodel due to an increase in the dimensionality of the PCA-space, it is possible to obtain metamodels of high accuracy.

A slight change in the dimensions of PCA-spaces, due to the values of eigenvalues, that were no more than the order of 10^{-3}, resulted in insignificant improvement in the accuracy of reconstructing material properties profiles. A slight increase in the dimensionality of the search space obviously somewhat complicates the conditions for finding an extremum in PCA-space, but the accuracy of its finding is slightly improved, while a considerable increase in its dimensionality leads to a more severe manifestation of the "curse of dimensionality" effect. In this case, the accuracy of profile search is lost. However, it makes sense to choose the smallest possible dimension of PCA-spaces, which ensures the uncomplicatedness and accuracy of surrogate models, and favorable conditions for finding an extremum during optimization.

As a result of numerical experiments, it was possible to find a certain compromise regarding the dimensionality of the reduced space based on the analysis of the accuracy of determining the near-surface distributions of the electrophysical material properties and the dimensionality of PCA-reduced surrogate models, which is observed at the level of 63 and at which the accuracy of profile identification by the RMAE indicator does not exceed 0.178% for MP and 0.204% for EC. At the same time, the maximum relative errors of profile measurement were 0.24% and 0.27%, respectively. It is interesting to note that the authors of the study obtained a solution to a similar inverse problem in the full factor space and showed the results of reconstructing the profiles of the MP and EC at the level of 5% error [23].

Thus, the computer experiments have convincingly demonstrated the capabilities of the proposed method for determining the profiles of material properties of planar TOs using surrogate optimization techniques in a reduced PCA-space and accumulating the most important a priori information about objects during eddy-current testing of their microstructural features.

The method of determining material property profiles proposed by the authors has prospects for its improvement. The use of inversion-capable neural networks, namely Invertible Neural Networks, looks quite attractive, as it makes it possible to avoid the application of the optimization iterative procedure to find profiles. Their use automatically solves the complex problem of a one-to-many relationship to form an unambiguous mapping in the original design space, which is characteristic of the entire class of inverse problems when overcoming any non-uniqueness of inverse solutions. In addition, it can be noted that the method is quite versatile, which, with minor modifications, can be used to solve inverse design problems in many fields of technology.

Author Contributions: Conceptualization, V.Y.H. and R.T.; methodology, V.Y.H. and R.T.; software, V.Y.H.; validation, R.T.; formal analysis, V.T.; investigation, R.T. and V.T.; resources, N.T.; data curation, V.T.; writing—original draft preparation, V.T. and N.T.; writing—review and editing, V.Y.H. and R.T.; visualization, N.T.; supervision, V.Y.H. and V.K.; project administration, V.Y.H. and V.K.; funding acquisition, V.K. All authors have read and agreed to the published version of the manuscript.

Funding: The work was performed free of charge with the support of the research work of Cherkasy State Technological University (Project #0122U200836).

Data Availability Statement: Most data are contained within the article. All the data are available on request due to restrictions, e.g., privacy or ethics.

Acknowledgments: The authors are grateful to all colleagues and institutions that contributed to the research and made it possible to publish its results.

Conflicts of Interest: The authors declare no conflicts of interest.

References

1. Campbell, S.D.; Werner, D.H. *Advances in Electromagnetics Empowered by Artificial Intelligence and Deep Learning*; John Wiley & Sons: Hoboken, NJ, USA, 2023.

2. Hampton, J.; Fletcher, A.; Tesfalem, H.; Peyton, A.; Brown, M. A comparison of non-linear optimisation algorithms for recovering the conductivity depth profile of an electrically conductive block using eddy current inspection. *NDT E Int.* **2022**, *125*, 102571. [CrossRef]
3. Xia, Z.; Huang, R.; Chen, Z.; Yu, K.; Zhang, Z.; Salas-Avila, J.R.; Yin, W. Eddy current measurement for planar structures. *Sensors* **2022**, *22*, 8695. [CrossRef] [PubMed]
4. Sabbagh, H.A.; Murphy, R.K.; Sabbagh, E.H.; Zhou, L.; Wincheski, R. *Advanced Electromagnetic Models for Materials Characterization and Nondestructive Evaluation*; Springer International Publishing: Heidelberg, Germany, 2021.
5. Lu, M.; Meng, X.; Huang, R.; Chen, L.; Peyton, A.; Yin, W. A high-frequency phase feature for the measurement of magnetic permeability using eddy current sensor. *NDT E Int.* **2021**, *123*, 102519. [CrossRef]
6. Lu, M.; Meng, X.; Huang, R.; Chen, L.; Peyton, A.; Yin, W. Measuring Lift-Off Distance and Electromagnetic Property of Metal Using Dual-Frequency Linearity Feature. *IEEE Trans. Instrum. Meas.* **2020**, *70*, 6001409. [CrossRef]
7. Huang, R.; Lu, M.; He, X.; Peyton, A.; Yin, W. Measuring coaxial hole size of finite-size metallic disk based on a dual-constraint integration feature using multifrequency eddy current testing. *IEEE Trans. Instrum. Meas.* **2020**, *70*, 6001007. [CrossRef]
8. Lu, M.; Meng, X.; Chen, L.; Huang, R.; Yin, W.; Peyton, A. Measurement of Ferromagnetic Slabs Permeability Based on a Novel Planar Triple-Coil Sensor. *IEEE Sens. J.* **2020**, *20*, 2904–2910. [CrossRef]
9. Lahrech, A.C.; Naidjate, M.; Helifa, B.; Zaoui, A.; Abdelhadi, B.; Lefkaier, I.-K.; Feliachi, M. Development of an axial rotating magnetic field multi-coil eddy current sensor for electromagnetic characterization of stratified CFRP materials. *NDT E Int.* **2022**, *126*, 102589. [CrossRef]
10. Meng, T.; Tao, Y.; Chen, Z.; Avila, J.R.S.; Ran, Q.; Shao, Y.; Huang, R.; Xie, Y.; Zhao, Q.; Zhang, Z.; et al. Depth evaluation for metal surface defects by eddy current testing using deep residual convolutional neural networks. *IEEE Trans. Instrum. Meas.* **2021**, *70*, 2515413. [CrossRef]
11. She, S.; Zheng, X.; Xiong, L.; Meng, T.; Zhang, Z.; Shao, Y.; Yin, W.; Shen, J.; He, Y. Thickness Measurement and Surface-defect Detection for Metal Plate Using Pulsed Eddy Current Testing and Optimized Res2Net Network. *IEEE Trans. Instrum. Meas.* **2024**, *73*, 2530313. [CrossRef]
12. Xia, Z.; Huang, R.; Lu, M.; Yin, W. Thickness and permeability estimation of metallic plates by triple-frequency eddy-current testing with probe lift-off. *IEEE Trans. Instrum. Meas.* **2023**, *73*, 6000208. [CrossRef]
13. Jin, Z.; Meng, Y.; Yu, R.; Huang, R.; Lu, M.; Xu, H.; Meng, X.; Zhao, Q.; Zhang, Z.; Peyton, A. Methods of controlling lift-off in conductivity invariance phenomenon for eddy current testing. *IEEE Access* **2020**, *8*, 122413–122421. [CrossRef]
14. Tesfalem, H.; Hampton, J.; Fletcher, A.D.; Brown, M.; Peyton, A.J. Electrical resistivity reconstruction of graphite moderator bricks from multi-frequency measurements and artificial neural networks. *IEEE Sens. J.* **2021**, *21*, 17005–17016. [CrossRef]
15. Hampton, J.; Tesfalem, H.; Dorn, O.; Fletcher, A.; Peyton, A.; Brown, M. Calibration of a Finite Element Forward Model in Eddy Current Inspection. *IEEE Sens. J.* **2022**, *22*, 10699–10707. [CrossRef]
16. Tesfalem, H.; Peyton, A.J.; Fletcher, A.D.; Brown, M.; Chapman, B. Conductivity profiling of graphite moderator bricks from multifrequency eddy current measurements. *IEEE Sens. J.* **2020**, *20*, 4840–4849. [CrossRef]
17. Xu, J.; Wu, J.; Xin, W.; Ge, Z. Measuring ultrathin metallic coating properties using swept-frequency eddy-current technique. *IEEE Trans. Instrum. Meas.* **2020**, *69*, 5772–5781. [CrossRef]
18. Xu, J.; Wu, J.; Xin, W.; Ge, Z. Fast measurement of the coating thickness and conductivity using eddy currents and plane wave approximation. *IEEE Sens. J.* **2020**, *21*, 306–314. [CrossRef]
19. Huang, P.; Zhao, J.; Li, Z.; Pu, H.; Ding, Y.; Xu, L.; Xie, Y. Decoupling Conductivity and Permeability Using Sweep-Frequency Eddy Current Method. *IEEE Trans. Instrum. Meas.* **2023**, *72*, 6001911. [CrossRef]
20. Hampton, J.; Tesfalem, H.; Fletcher, A.; Peyton, A.; Brown, M. Reconstructing the conductivity profile of a graphite block using inductance spectroscopy with data-driven techniques. In *Insight-Non-Destructive Testing and Condition Monitoring*; The British Institute of Non-Destructive Testing: Northampton, UK, 2021; Volume 63, pp. 82–87.
21. Theodoulidis, T.P.; Kriezis, E.E. *Eddy Current Canonical Problems (with Applications to Nondestructive Evaluation)*; Tech Science Press: Henderson, NV, USA, 2006.
22. Halchenko, V.Y.; Tychkov, V.V.; Storchak, A.V.; Trembovetska, R.V. Reconstruction of surface radial profiles of electrophysical characteristics of cylindrical objects during eddy current measurements with a priori data. The selection formation for the surrogate model construction. *Ukr. Metrol. J.* **2020**, *1*, 35–50.
23. Halchenko, V.Y.; Trembovetska, R.; Tychkov, V.; Tychkova, N. Surrogate methods for determining of profiles of material properties of planar test objects with accumulation of apriori information about them. *Archives Electr. Eng.* **2024**, *73*, 183–200. [CrossRef]
24. Halchenko, V.Y.; Trembovetska, R.; Tychkov, V.; Tychkova, N. The inverse problem of determining of electrophysical parameters profiles in eddy-current structuroscopy using apriori information on multifrequency sensing. *Math. Model. Anal.* **2024**, *29*, 767–780. [CrossRef]
25. Halchenko, V.Y.; Trembovetska, R.; Tychkov, V.; Tychkova, N. Reconstruction of electrophysical parameters distribution during eddy current measurements of structural features of planar metal objects. *Latv. J. Phys. Tech. Sci.* **2024**, *61*, 61–75. [CrossRef]

26. Jiang, P.; Zhou, Q.; Shao, X. *Surrogate-Model-Based Design and Optimization*; Springer: Singapore, 2020; pp. 135–236.
27. Halchenko, V.Y.; Storchak, A.; Trembovetska, R.; Tychkov, V. The creation of a surrogate model for restoring surface profiles of the electrophysical characteristics of cylindrical objects. *Ukr. Metrol. J.* **2020**, *3*, 27–35.
28. Kundu, T. Recent Developments in Non-destructive Testing. In *Earthquake Resistant Design, Protection, and Performance Assessment in Earthquake Engineering*; Springer Nature: Berlin, Germany, 2024; Volume 54, p. 165.
29. Xia, Z.; Yan, J.; Huang, R.; Lu, M.; Cui, Z.; Peyton, A.; Yin, W.; Yang, W. Fast estimation of metallic pipe properties using simplified analytical solution in eddy-current testing. *IEEE Trans. Instrum. Meas.* **2022**, *72*, 1000513. [CrossRef]
30. Patnaik, A.; Kukshal, V.; Agarwal, P.; Sharma, A.; Choudhary, M. *Application of Soft Computing Techniques in Mechanical Engineering*; CRC Press: Boca Raton, FL, USA, 2022.
31. Alswaitti, M.; Siddique, K.; Jiang, S.; Alomoush, W.; Alrosan, A. Dimensionality Reduction, Modelling, and Optimization of Multivariate Problems Based on Machine Learning. *Symmetry* **2022**, *14*, 1282. [CrossRef]
32. Ullah, S.; Nguyen, D.A.; Wang, H.; Menzel, S.; Sendhoff, B.; Bäck, T. Exploring dimensionality reduction techniques for efficient surrogate-assisted optimization. In Proceedings of the 2020 IEEE Symposium Series on Computational Intelligence (SSCI), Canberra, ACT, Australia, 1–4 December 2020; pp. 2965–2974.
33. Diaz-Papkovich, A.; Anderson-Trocmé, L.; Gravel, S. A review of UMAP in population genetics. *J. Hum. Genet.* **2021**, *66*, 85–91. [CrossRef]
34. Ghojogh, B.; Ghodsi, A.; Karray, F.; Crowley, M. Uniform Manifold approximation and projection (UMAP) and its variants: Tutorial and survey. *arXiv* **2021**, arXiv:2109.02508.
35. Su, B.; Li, Y.; Liu, Z.; Wang, J.; Chen, Z. Near- and remote-field pulsed eddy current integrated testing for enhancement in imaging of buried flaws in layered conductive structures. *Nondestruct. Test. Eval.* **2024**, 1–14. [CrossRef]
36. Uchanin, V.M. Surface eddy current probes of double differential type as an effective tool to solve non-destructive inspection problems. *Paton Weld. J.* **2023**, *2*, 46–55. [CrossRef]
37. Ribichini, R.; Giolli, C.; Scrinzi, E. Eddy-Current Evaluation of Platinum Aluminide Coatings. In Proceedings of the 50th Annual Review of Progress in Quantitative Nondestructive Evaluation American Society of Mechanical Engineer, Austin, TX, USA, 24–27 July 2023.
38. Uzal, E. Theory of Eddy Current Inspection of Layered Metals. Ph.D. Thesis, Iowa State University, Ames, IA, USA, 1992.
39. Trembovetska, R.; Halchenko, V.; Bazilo, C. Inverse multi-parameter identification of plane objects electrophysical parameters profiles by eddy-current method. In *International Conference on Smart Technologies in Urban Engineering*; Springer International Publishing: Cham, Switzerland, 2022; Volume 536, pp. 202–212.
40. Halchenko, V.; Trembovetska, R.; Bazilo, C.; Tychkova, N. Computer Simulation of the Process of Profiles Measuring of Objects Electrophysical Parameters by Surface Eddy Current Probes. In *International Scientific-Practical Conference "Information Technology for Education, Science and Technics"*; Springer Nature: Cham, Switzerland, 2022; Volume 178, pp. 411–424.
41. Halchenko, V.; Trembovetska, R.; Tychkov, V.; Tychkova, N. Construction of Quasi-DOE on Sobol's Sequences with Better Uniformity 2D Projections. *Appl. Comput. Syst.* **2023**, *28*, 21–34. [CrossRef]
42. Taheri, H.; Gonzalez Bocanegra, M.; Taheri, M. Artificial intelligence, machine learning and smart technologies for nondestructive evaluation. *Sensors* **2022**, *22*, 4055. [CrossRef]
43. Ledolter, J.; Kardon, R.H. Focus on data: Statistical design of experiments and sample size selection using power analysis. *Investig. Ophthalmol. Vis. Sci.* **2020**, *61*, 11. [CrossRef] [PubMed]
44. Yao, Y.; Wang, H. *A Selective Review on Statistical Techniques for Big Data*; Springer Nature: Cham, Switzerland, 2021.
45. Kuznetsov, B.; Bovdui, I.; Nikitina, T. Optimal Design of System of Active Shielding of Magnetic Field Generated by Overhead Power Lines. In Proceedings of the 2021 IEEE 16th International Conference on the Experience of Designing and Application of CAD Systems (CADSM), Lviv, Ukraine, 22–26 February 2021.
46. Koshevoy, N.D.; Kirichenko, A.L.; Borisenko, S.A.; Muratov, V.V. Research and optimization of the influence of fractional composition of the working mixture of powders on the characteristics of the solid mixture fuel. *Aerosp. Tech. Technol.* **2020**, *162*, 42–52.